Physics Letters A 414 (2021) 127607

Contents lists available at ScienceDirect

Physics Letters A

www.elsevier.com/locate/pla

Metallic nature and site-selective magnetic moment collapse in iron oxide Fe_4O_5 at the extreme conditions of Earth's deep interior

Aiqin Yang [1], Qiaoying Qin [1], Xiangru Tao, Shengli Zhang, Yongtao Zhao *, Peng Zhang **

MOE Key Laboratory for Nonequilibrium Synthesis and Modulation of Condensed Matter, School of Physics, Xi'An Jiaotong University, Xi'An 710049, China

ARTICLE INFO

Article history:
Received 1 June 2021
Received in revised form 29 July 2021
Accepted 29 July 2021
Available online 9 August 2021
Communicated by L.M. Woods

Keywords:
Fe_4O_5
Extreme conditions
Magnetic moment collapse
DFT+DMFT

ABSTRACT

Properties of iron oxides at the extreme conditions are of essential importance in condensed matter physics and Geophysics. The recent discovery of a new type of iron oxide, Fe_4O_5, at high pressure and high temperature of Earth's deep interior attracts great interests. In this paper, we report the electronic structure and the magnetic properties of Fe_4O_5 employing the density functional theory plus dynamic mean field theory (DFT+DMFT) approach. We find that Fe_4O_5 stays metallic from ambient pressure to high pressure. The magnetic moments of iron atoms at the three different crystallographic positions of Fe_4O_5 undergo position-dependent collapse as being compressed. Such site-selective magnetic moment collapse originates from the shift of energy levels and the consequent charge transfer among the Fe-3*d* orbits under compression.

1. Introduction

Iron oxides that consist of the two most abundant elements on Earth are important components of Earth's mantle [1–8]. They account for about 7.5% of Earth's mass, only next to silicon and magnesium oxides. The electronic and the thermal conductivity of iron oxides are crucial for modeling the mantle of Earth and the interiors of other planets with compositions of iron and oxygen [9–11]. Iron oxides have also been widely used in industry [12,13] and biomedicine [14]. Therefore their properties have long attracted extensive interests of scientific communities.

Earth's mantle is in a high temperature, high pressure state. Typically, the temperature ranges from 500 K to 3000 K and the pressure ranges from 20 GPa to 140 GPa. At such extreme conditions, the oxidation states, the spin states and the phase stabilities of iron oxides may alter according to the environment [15,16]. The exploration of their properties at Earth's deep interior is imperative to understand the seismic observation and dynamic processes of Earth's mantle and outer core [3,7,8,17–19]. At the ambient conditions, there are three known forms of iron oxides including wüstite (FeO), magnetite (Fe_3O_4), hematite (Fe_2O_3) [2,7,12,13,15,19,20]. Recently, a series of new iron oxides were identified at high pressure and high temperature including FeO_2 [5,8,19,21], Fe_4O_5 [9,15], Fe_5O_6 [4,22], Fe_5O_7 [21], Fe_7O_9 [23] and $Fe_{13}O_{19}$ [24]. In 2011, Lavina et al. firstly reported the synthesis of a stoichiometric iron oxide Fe_4O_5 at 10 GPa and 1800 K [15]. Fe_4O_5 possesses a $CaFe_3O_5$-type crystal structure with space group *Cmcm* [3,7,15,25]. Its atomic arrangement can be viewed as a stacking along the *c*-axis of layers of edge-sharing FeO_6 octahedra with two slightly different iron positions Fe1 (4*a* site) and Fe2 (8*f* site), and layers of face-sharing trigonal prisms with the third iron position Fe3 (4*c* site) (see Fig. 1).

The discovery of Fe_4O_5 immediately stimulates great interests in exploring the properties this new iron oxide since it is energetically more favorable with increased pressures than stoichiometric Fe_3O_4 and FeO [2]. This opens up the possibility that Fe_4O_5 could be stable in Earth's mantle. Density functional theory calculations suggest an antiferromagnetic ground state for Fe_4O_5 [3]. Experiments by Ovsyannikov et al. indicate an unusual charge-ordering transition in Fe_4O_5 at about 150 K, resulting from competing formation of Fe dimer and trimer [25]. Later they further determined the phase diagram of Fe_4O_5 at high pressures and low temperatures, pointing out that the charge ordering can be tuned by pressure [7]. However, the investigation of Fe_4O_5 at high pressures and high temperatures, which is of critical importance for the modeling of Earth's mantle, is totally absent. In this letter we will present a DFT+DMFT [26] calculation of the electronic and the magnetic properties of the strongly correlated material at the high temperature and high pressure conditions of Earth's deep interior.

* Corresponding author.
** Principal corresponding author.
E-mail addresses: zhaoyongtao@xjtu.edu.cn (Y. Zhao), zpantz@xjtu.edu.cn (P. Zhang).
[1] A.Q. Y. and Q.Y. Q. contributed equally to this work.

https://doi.org/10.1016/j.physleta.2021.127607
0375-9601/

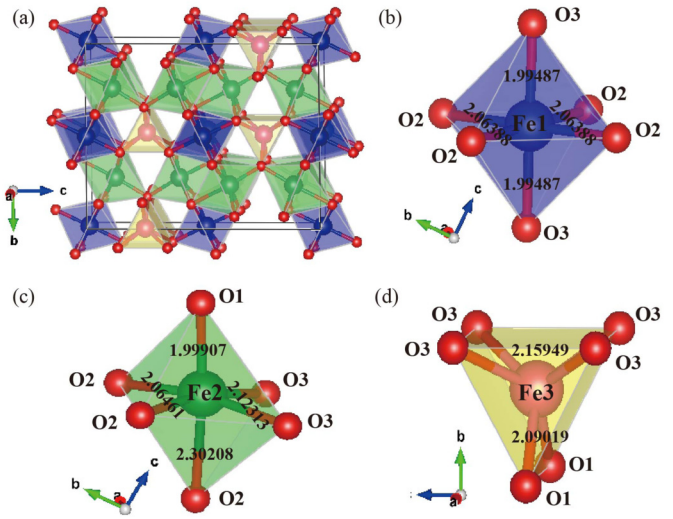

Fig. 1. (Color online.) Crystal structure of Fe_4O_5 (a), FeO_6 octahedra (b-c) and FeO_6 trigonal prisms (d). The blue and green octahedra show the local coordination of sites Fe1 (4*a*) and Fe2 (8*f*) and the yellow trigonal prism shows the local coordination of site Fe3 (4*c*). The bond lengths at the ambient conditions are marked in the subfigures.

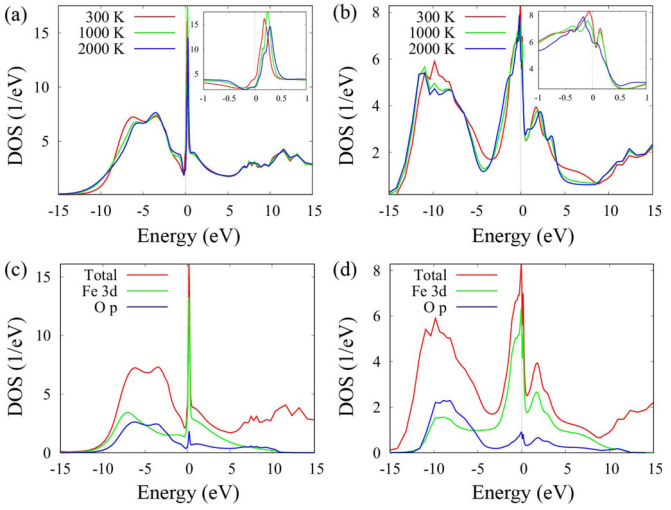

Fig. 2. (Color online.) The total density of states (DOS) of Fe_4O_5 at the ambient pressure (a) and at 45% volume compression (b) at temperatures of 300 K, 1000 K and 2000 K. The insets show the DOS of Fe_4O_5 in energy window [-1 eV, 1 eV]. The orbital-projected DOS of Fe_4O_5 at 300 K, the ambient pressure (c) and at 300 K, 45% volume compression (d).

2. Computational methods

The DFT+DMFT method. In DFT+DMFT calculation, first we adopt the all electron LAPW Wien2k package [27] in the DFT part to get converged charge density, eigenvectors and eigenenergies of the Kohn-Sham equations. We choose the Wu-Cohen [28] exchange correlation function and a 20×20×4 *k*-point mesh. The cutoff energy is -6.0 Ry and $R_{mt}\cdot K_{max}$ = 7, where R_{mt} is the smallest atomic sphere radius in the unit cell and K_{max} is the magnitude of the largest K vector. The smallest atomic radius of Fe is 1.65 bohr and that of O is 1.42 bohr at the 45% volume compression. The DFT convergence criteria of charge and energy are set as 1×10^{-5} *e* and 1×10^{-5} Ry respectively. In the DMFT [29] part, the hybridization expansion continuous time quantum Monte Carlo (CTQMC) [30,31] is used as the impurity solver of the DMFT self-consistent equations to get the self-energy. A total number of 10^7 Monte Carlo updates are used in the DMFT iteration. After the converged DMFT iterations, the charge density is updated and then being used to construct the new Kohn-Sham potential for the next DFT iterations. In the Supplementary Information Fig. S1-S2, we presented the evolution of the self-energy and the Green's function with respect to the DMFT iterations for the five Fe-3*d* orbits of the three different iron atoms at 300 K and at the ambient pressure. After 30 DMFT iterations, the DFT+DMFT calculations stop when we have reached fully convergence of the self-energy and the Green's function. The double counting energy is calculated from the fully localized limit method [32]. The DFT+DMFT calculated self-energy on the imaginary axis is rotated to the real axis by the maximum entropy analytical continuation method [33].

Coulomb interaction U and Hund's coupling J. In the CTQMC part, the requested screened Coulomb interaction U and the Hund's coupling J of the Fe-3*d* orbitals are determined by the constrained density functional theory (cDFT) method [34]. There are three nonequivalent iron atoms Fe1 (4*a* site), Fe2 (8*f* site) and Fe3 (4*c* site) in $CaFe_3O_5$-type Fe_4O_5. We calculated the Coulomb U and the Hund's J at both V_0 = 603.86 $bohr^3/Fe_4O_5$ (volume per formula unit at the ambient pressure, *a* = 5.473443 bohr, *b* = 18.561956 bohr, *c* = 23.774408 bohr) and V = 572.13 $bohr^3/Fe_4O_5$ (in later text note as $(1\text{-}V/V_0)\%$ = 5.25% compression). At the ambient pressure U, J = 6.81 eV, 0.89 eV at Fe1, 6.42 eV, 0.9 eV at Fe2, and 6.91 eV, 0.94 eV at Fe3. At 5.25% compression U, J = 6.53 eV, 0.88 eV at Fe1, 6.35 eV, 0.9 eV at Fe2, and 6.82 eV, 0.94 eV at Fe3. Since the value of the Coulomb interaction U and the Hund's coupling J is not very sensitive to position and compression, we choose U, J = 6.7 eV, 0.9 eV throughout our calculations at every volume and temperature for all Fe-3*d* electrons. We also tested U = 5 eV and 10 eV, J = 0.7 eV and 1.12 eV at the ambient pressure. The different values of U, J only slightly change the derived charge density, density of states *etc.*, but all conclusions we presented in this letter stay valid.

The pressure-volume relationship. Based on our DFT + DMFT calculation of the total energy-volume relationship of Fe_4O_5 at 300 K, we are able to derive the pressure-volume dependence as presented in the Supplementary Information Fig. S3. Our numerical curve reasonably overlaps the powder x-ray diffraction data by Lavina et al. [15] below 30 GPa.

3. Results and discussions

At the ambient conditions, some iron oxides including FeO and Fe_2O_3 are Mott-type insulators, while magnetite Fe_3O_4 is metal. Our DFT+DMFT calculations indicate that the electronic conduction property of Fe_4O_5 is close to Fe_3O_4. The total and the orbital-projected density of state (DOS) of Fe_4O_5 are presented in Fig. 2. In Fig. 2(a) and Fig. 2(b), the peak of the DOS at the Fermi level E_F clearly reveals the metallic nature of Fe_4O_5 from the ambient pressure to high pressures. As shown in Fig. 2(c) and Fig. 2(d), the total DOS of Fe_4O_5 at the Fermi level E_F has dominant Fe-3*d* character and minor O-*p* character that suggests the conduction in Fe_4O_5 is mainly due to the Fe-3*d* electrons. In Fig. 2(c) the sharp excitation peaks at about 0.2 eV above E_F indicate the Kondo screening of the itinerant O-*p* electrons by the heavy Fe-3*d* electrons. In the Supplementary Information Fig. S4 we present the hybridization function among the Fe-3*d* electrons and the conduction bath at 300 K and the ambient pressure. The hybridization peaks at E_F+0.2 eV for each Fe-3*d* orbits provide clear evidence of the strong hybridization among the conduction electrons and the Fe-3*d* electrons that form the local magnetic moments. Such Kondo scattering is also observed in other transition metal oxides like FeO, MnO, CoO and NiO [35–37]. At 45% volume compression in Fig. 2(d) the peak is lower due to band broadening.

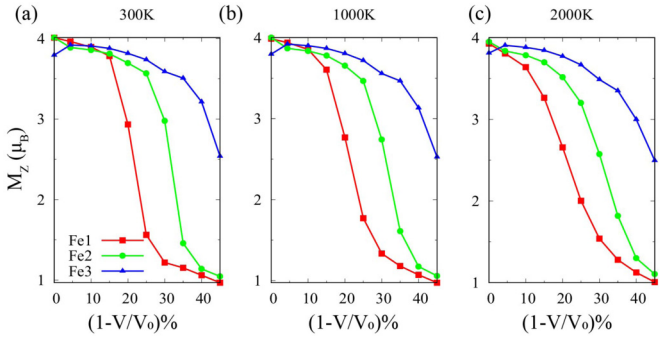

Fig. 3. (Color online.) The magnetic moments of Fe_4O_5 at 300 K (a), 1000 K (b) and 2000 K (c) as a function of compression. Red square represents the magnetic moment of Fe1 (4*a*), the green circle represents the magnetic moment of Fe2 (8*f*), and the blue triangle represents the magnetic moment of Fe3 (4*c*). (1-V/V_0)% is the notation of volume compression percentage, where V_0 = 603.86 $bohr^3/Fe_4O_5$ is the volume per formula unit at the ambient pressure.

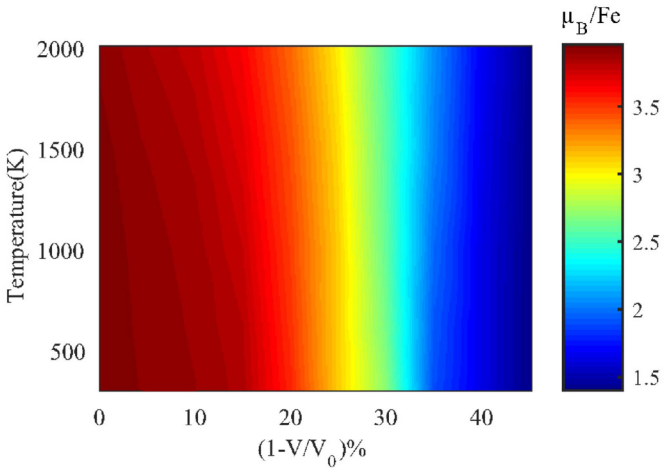

Fig. 4. (Color online.) The average magnetic moment of iron versus temperature and pressure in Fe_4O_5. Color indicates the value of magnetic moment in unit of μ_B/Fe.

Previous first-principles calculations suggest magnetic moments of Fe atoms in range of ∼3.6-3.8 μ_B/Fe in the pressure range of 0-30 GPa [3]. However, our DFT+DMFT calculations indicate that the local magnetic moments $\sqrt{\langle m_z^2 \rangle}$ in Fe_4O_5 undergo site-selective magnetic collapse under compression as shown in Fig. 3. In Fig. 3, the magnetic moments of all three iron atoms are around 3.8-4.0 μ_B/Fe at the ambient pressure. As Fe_4O_5 is compressed, the magnetic moment of Fe1 (4*a*) decreases firstly, then that of Fe2 (8*f*) decreases secondly, and that of Fe3 (4*c*) decreases lastly. At 45% compression endpoint, the magnetic moments of Fe1 (4*a*) and Fe2 (8*f*) saturate at about 1.0 μ_B/Fe, while the magnetic moment of Fe3 (4*c*) is about 2.5 μ_B/Fe. In addition, we also noticed that the magnetic moment of Fe1 (4*a*) at 300 K decreases at relative higher speed than that at 2000 K. Such temperature tuned speed of magnetic moment collapse is not that obvious at Fe2 (8*f*) and the temperature effect seems to disappear at Fe3 (4*c*). The evolution of the average magnetic moment of iron atoms at the three sites as a function of pressure and temperature is summarized in Fig. 4. Although in Fig. 4 the temperature effect is less significant, we still find that the speed of magnetic moment collapses gradually slow down as raising temperatures, especially in the red color region. Similar site-selective magnetic moment collapse has also been observed in Fe_5O_6 [22].

In transition metal oxides like FeO, Fe_2O_3 and MnO their high spin-low spin transitions coexist with the insulator-metal transitions [38–40]. Thus the insulator-metal transitions in these materials are often presumed originate from the spin fluctuations. Here in metallic Fe_4O_5 we find the site-selective spin transition could be independent of the electronic insulator-metal transition. Such behavior has also been observed in FeO_2, where they find a spin transition at about 14 GPa in contrast FeO_2 always stay metallic without pressure driven insulator-metal transition [41].

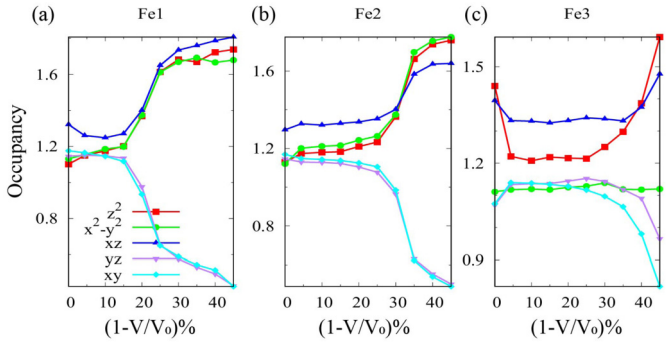

Fig. 5. (Color online.) The compression dependent electron occupancies of five Fe-3*d* orbits at 300 K at Fe1 (4*a*), Fe2 (8*f*), and Fe3 (4*c*) in panels (a)-(c) respectively.

Previous works on transition metal mono-oxides prove that the collapse of magnetic moment is related to the partition of electrons of the *d*-orbit in transition metals [40,42]. We calculate the electron occupancies on the five Fe-3*d* orbits at three crystallographic sites Fe1 (4*a*), Fe2 (8*f*) and Fe3 (4*c*) at 300 K. As shown in Fig. 5, at Fe1 (4*a*) and Fe2 (8*f*) positions the electron occupancies of the z^2, x^2-y^2 and xz orbits increase at compression of volume, while the electron occupancies of the yz and xy orbits decrease. It indicates the transfer of electrons from the yz, xy orbits to the z^2, x^2-y^2, xz orbits of iron at compression. However, the change of the electron occupancies at the 4*c* position is less significant, which indicates that the electronic correlations of Fe3 atom are stronger relative to the electronic correlations of Fe1 and Fe2. The analysis of the bond lengths of the iron atoms at three crystallographic positions with the surrounding oxygen atoms further confirms this view. As shown in Fig. 1, the Fe-O bonds in the trigonal prism around Fe3 (4*c*) are longer than the Fe-O bonds in the octahedra around Fe1 (4*a*) and Fe2 (8*f*), indicating that the electrons in the trigonal prism are more localized.

Such electron partitioning incurred magnetic moment collapse scenario can be understood in a simplified picture. At the ambient condition all five Fe-3*d* orbits are almost evenly occupied and the Hund's rule maximized the magnetic moments at around 4.0 μ_B/Fe. At the extreme compression condition imagining that all electrons of the yz, xy orbits have been transferred to the z^2, x^2-y^2, xz orbits, then the six Fe-3*d* electrons must be pairing in singlets due to the Pauli exclusion principle and the total magnetic moment is zero.

The transfer of electrons among the five Fe-3*d* orbits originates from the shift of energy levels of these orbits under compression. The energy difference of the x^2-y^2, xz, yz and xy orbits relative to the z^2 orbit under compression is shown in Fig. 6. Under compression, energies of the yz and the xy orbits at Fe1 (4*a*) and Fe2 (8*f*) sites move upward while energies of the z^2, x^2-y^2, and xz orbits stay almost invariant. Then electrons on the yz and xy orbits transfer to the z^2, x^2-y^2, and xz orbits in order to minimize the total energy in Fe_4O_5 crystal. In contrast, the orbital-energy differences of the Fe3 (4*c*) site increase much slower under compression, which leads to the slow magnetic moment collapse at the Fe3 (4*c*) site in Fig. 3.

4. Conclusion

Our study shows that Fe_4O_5 of $CaFe_3O_5$-type is always metallic from the ambient pressure to high pressures. Under compres-

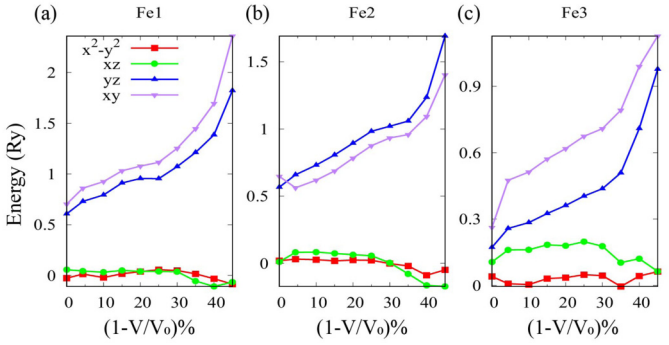

Fig. 6. (Color online.) Pressure dependence of energy difference among the $x^2 - y^2$, xz, yz and xy orbits relative to the z^2 orbit at Fe1 ($4a$), Fe2 ($8f$) and Fe3 ($4c$) at 300 K in panels (a)-(c) respectively.

sion the three non-equivalent iron atoms in Fe_4O_5 exhibit site-dependent collapse of magnetic moments. The magnetic moments of iron at Fe1 ($4a$ site) and Fe2 ($8f$ site) collapse from about 4.0 μ_B/Fe at the ambient pressure to about 1.0 μ_B/Fe at 45% compression. But the magnetic moment of iron at Fe3 ($4c$ site) decreases much slower since it has the strongest electron correlations among the three non-equivalent iron sites in Fe_4O_5. By further calculation of the electron occupancies and the energy levels of the five Fe-3d orbits, we prove that the site-selective magnetic collapse in Fe_4O_5 results from the shift of orbital energies and the charge transfer among these orbits under compression. Our calculations indicate high conductivity and possible volume collapse in Fe_4O_5 at the extreme conditions, which will affect the dynamics in Earth's deep interior such as the energy exchange and the mass partition at the core-mantle boundary.

CRediT authorship contribution statement

Aiqin Yang: Software, Data curation & analysis, Original draft preparation, Review & Editing.

Qiaoying Qin: Software, Data curation.

Xiangru Tao: Software, Visualization.

Shengli Zhang: Supervision, Conceptualization.

Yongtao Zhao: Supervision, Writing – review & editing.

Peng Zhang: Supervision, Conceptualization, Methodology, Writing – review & editing.

Declaration of competing interest

The authors declare that they have no known competing financial interests or personal relationships that could have appeared to influence the work reported in this paper.

Acknowledgements

A.Q. Y., Q.Y. Q. and P. Z. acknowledge the support of National Natural Science Foundation of China No. 11604255 and the Natural Science Basic Research Program of Shaanxi No. 2021JM-001. Y. T. Z. acknowledges the support of National Key R & D Program of China under Grant No. 2019YFA0404900, the Science Challenge Project under Grant No. TZ2016005. This work is also supported by the HPC platform of Xi'an Jiaotong University.

Appendix A. Supplementary material

Supplementary material related to this article can be found online at https://doi.org/10.1016/j.physleta.2021.127607.

References

[1] K. Otsuka, S.-I. Karato, Deep penetration of molten iron into the mantle caused by a morphological instability, Nature (London) 492 (2012) 243–246.
[2] J. Guignard, W.A. Crichton, Synthesis and recovery of bulk Fe_4O_5 from magnetite, Fe_3O_4. A member of a self-similar series of structures for the lower mantle and transition zone, Mineral. Mag. 78 (2014) 361–371.
[3] K. Kothapalli, E. Kim, T. Kolodziej, P.F. Weck, E.E. Alp, Y. Xiao, P. Chow, C. Kenney-Benson, Y. Meng, S. Tkachev, et al., Nuclear forward scattering and first-principles studies of the iron oxide phase Fe_4O_5, Phys. Rev. B 90 (2014) 024430.
[4] B. Lavina, Y. Meng, Unraveling the complexity of iron oxides at high pressure and temperature: synthesis of Fe_5O_6, Sci. Adv. 1 (2015).
[5] G.L. Weerasinghe, C.J. Pickard, R.J. Needs, Computational searches for iron oxides at high pressures, J. Phys. Condens. Matter 27 (2015) 455501.
[6] F. Lagroix, S.K. Banerjee, M.J. Jackson, Geological Occurrences and Relevance of Iron Oxides, Wiley-VCH, Weinheim, 2016, pp. 7–30.
[7] S.V. Ovsyannikov, M. Bykov, E. Bykova, K. Glazyrin, R.S. Manna, A.A. Tsirlin, V. Cerantola, I. Kupenko, A.V. Kurnosov, I. Kantor, et al., Pressure tuning of charge ordering in iron oxide, Nat. Commun. 9 (2018) 4142.
[8] C. Lu, M. Amsler, C. Chen, Unraveling the structure and bonding evolution of the newly discovered iron oxide FeO_2, Phys. Rev. B 98 (2018) 054102.
[9] A.B. Woodland, D.J. Frost, D.M. Trots, K. Klimm, M. Mezouar, In situ observation of the breakdown of magnetite (Fe_3O_4) to Fe_4O_5 and hematite at high pressures and temperatures, Am. Mineral. 97 (2012) 1808–1811.
[10] C. Lu, C. Chen, High-pressure evolution of crystal bonding structures and properties of FeOOH, J. Phys. Chem. Lett. 9 (2018) 2181–2185.
[11] J. Zhang, J. Lv, H. Li, X. Feng, C. Lu, S.A.T. Redfern, H. Liu, C. Chen, Y. Ma, Rare helium-bearing compound FeO_2He stabilized at deep-Earth conditions, Phys. Rev. Lett. 121 (2018) 255703.
[12] C. Xia, Y. Jia, M. Tao, Q. Zhang, Tuning the band gap of hematite α-Fe_2O_3 by sulfur doping, Phys. Lett. A 377 (2013) 1943–1947.
[13] W. Lei, Y. Liu, X. Si, J. Xu, W. Du, J. Yang, T. Zhou, J. Lin, Synthesis and magnetic properties of octahedral Fe_3O_4 via a one-pot hydrothermal route, Phys. Lett. A 381 (2017) 314–318.
[14] A.K. Gupta, M. Gupta, Synthesis and surface engineering of iron oxide nanoparticles for biomedical applications, Biomaterials 26 (2005) 3995–4021.
[15] B. Lavina, P. Dera, E. Kim, Y. Meng, R.T. Downs, P.F. Weck, S.R. Sutton, Y. Zhao, Discovery of the recoverable high-pressure iron oxide Fe_4O_5, Proc. Natl. Acad. Sci. USA 108 (2011) 17281–17285.
[16] Q. Hu, D.Y. Kim, W. Yang, L. Yang, Y. Meng, L. Zhang, H.-K. Mao, FeO_2 and FeOOH under deep lower-mantle conditions and Earth's oxygen-hydrogen cycles, Nature (London) 534 (2016) 241–244.
[17] B.G. Jang, J. Liu, Q. Hu, K. Haule, H.-K. Mao, W.L. Mao, D.Y. Kim, J.H. Shim, Electronic spin transition in FeO_2: evidence for Fe(II) with peroxide O_2^{2-}, Phys. Rev. B 100 (2019) 014418.
[18] E. Bykova, L. Dubrovinsky, N. Dubrovinskaia, M. Bykov, C. McCammon, S. Ovsyannikov, H.-P. Liermann, I. Kupenko, A. Chumakov, R. Rüffer, et al., Structural complexity of simple Fe_2O_3 at high pressures and temperatures, Nat. Commun. 7 (2016) 10661.
[19] B.G. Jang, D.Y. Kim, J.H. Shim, Metal-insulator transition and the role of electron correlation in FeO_2, Phys. Rev. B 95 (2017) 075144.
[20] L.S. Darken, R.W. Gurry, The system iron-oxygen. I. The wüstite field and related equilibria, J. Am. Chem. Soc. 67 (1945) 1398–1412.
[21] X.-L. Zhang, Z.-W. Niu, M. Tang, J.-Z. Zhao, L.-C. Cai, First-principles thermoelasticity and stability of pyrite-type FeO_2 under high pressure and temperature, J. Alloys Compd. 719 (2017) 42–46.
[22] Q. Qin, A. Yang, X. Tao, L. Yang, H. Gou, P. Zhang, Site-selective magnetic moment collapse in compressed Fe_5O_6, Chin. Phys. Lett. 38 (2021) 089101.
[23] R. Sinmyo, E. Bykova, S.V. Ovsyannikov, C. McCammon, I. Kupenko, L. Ismailova, L. Dubrovinsky, Discovery of Fe_7O_9: a new iron oxide with a complex monoclinic structure, Sci. Rep. 6 (2016) 32852.
[24] M. Merlini, M. Hanfland, A. Salamat, S. Petitgirard, H. Müller, The crystal structures of $Mg_2Fe_2C_4O_{13}$, with tetrahedrally coordinated carbon, and $Fe_{13}O_{19}$, synthesized at deep mantle conditions, Am. Mineral. 100 (2015) 2001–2004.
[25] S.V. Ovsyannikov, M. Bykov, E. Bykova, D.P. Kozlenko, A.A. Tsirlin, A.E. Karkin, V.V. Shchennikov, S.E. Kichanov, H. Gou, A.M. Abakumov, et al., Charge-ordering transition in iron oxide Fe_4O_5 involving competing dimer and trimer formation, Nat. Chem. 8 (2016) 501–508.
[26] G. Kotliar, S.Y. Savrasov, K. Haule, V.S. Oudovenko, O. Parcollet, C.A. Marianetti, Electronic structure calculations with dynamical mean-field theory, Rev. Mod. Phys. 78 (2006) 865–951.
[27] P. Blaha, K. Schwarz, G. Madsen, D. Kvasnicka, J. Luitz, An Augmented Plane Wave Plus Local Orbitals Program for Calculating Crystal Properties, Vienna University of Technology, Austria, 2001.
[28] Z. Wu, R.E. Cohen, More accurate generalized gradient approximation for solids, Phys. Rev. B 73 (2006) 235116.
[29] A. Georges, G. Kotliar, W. Krauth, M.J. Rozenberg, Dynamical mean-field theory of strongly correlated fermion systems and the limit of infinite dimensions, Rev. Mod. Phys. 68 (1996) 13–125.

[30] P. Werner, A. Comanac, L. de' Medici, M. Troyer, A.J. Millis, Continuous-time solver for quantum impurity models, Phys. Rev. Lett. 97 (2006) 076405.
[31] K. Haule, Quantum Monte Carlo impurity solver for cluster dynamical mean-field theory and electronic structure calculations with adjustable cluster base, Phys. Rev. B 75 (2007) 155113.
[32] V.I. Anisimov, F. Aryasetiawan, A.I. Lichtenstein, First-principles calculations of the electronic structure and spectra of strongly correlated systems: the LDA+U method, J. Phys. Condens. Matter 9 (1997) 767–808.
[33] M. Jarrell, J. Gubernatis, Bayesian inference and the analytic continuation of imaginary-time quantum Monte Carlo data, Phys. Rep. 269 (1996) 133–195.
[34] G.K.H. Madsen, P. Novák, Charge order in magnetite. An LDA+U study, Europhys. Lett. 69 (2005) 777–783.
[35] J. Bała, A.M. Oleś, J. Zaanen, Zhang-Rice localization, quasiparticle dispersions, and the photoemission of NiO, Phys. Rev. Lett. 72 (1994) 2600–2603.
[36] J. Kuneš, V.I. Anisimov, S.L. Skornyakov, A.V. Lukoyanov, D. Vollhardt, NiO: correlated band structure of a charge-transfer insulator, Phys. Rev. Lett. 99 (2007) 156404.
[37] Q. Yin, A. Gordienko, X. Wan, S.Y. Savrasov, Calculated momentum dependence of Zhang-Rice states in transition metal oxides, Phys. Rev. Lett. 100 (2008) 066406.
[38] I. Leonov, Metal-insulator transition and local-moment collapse in FeO under pressure, Phys. Rev. B 92 (2015) 085142.
[39] E. Greenberg, I. Leonov, S. Layek, Z. Konopkova, M.P. Pasternak, L. Dubrovinsky, R. Jeanloz, I.A. Abrikosov, G.K. Rozenberg, Pressure-induced site-selective Mott insulator-metal transition in Fe_2O_3, Phys. Rev. X 8 (2018) 031059.
[40] J. Kuneš, A.V. Lukoyanov, V.I. Anisimov, R.T. Scalettar, W.E. Pickett, Collapse of magnetic moment drives the Mott transition in MnO, Nat. Mater. 7 (2008) 198–202.
[41] E. Koemets, I. Leonov, M. Bykov, E. Bykova, S. Chariton, G. Aprilis, T. Fedotenko, S. Clément, J. Rouquette, J. Haines, V. Cerantola, K. Glazyrin, C. McCammon, V.B. Prakapenka, M. Hanfland, H.-P. Liermann, V. Svitlyk, R. Torchio, A.D. Rosa, T. Irifune, A.V. Ponomareva, I.A. Abrikosov, N. Dubrovinskaia, L. Dubrovinsky, Revealing the complex nature of bonding in the binary high-pressure compound FeO_2, Phys. Rev. Lett. 126 (2021) 106001.
[42] R.E. Cohen, I.I. Mazin, D.G. Isaak, Magnetic collapse in transition metal oxides at high pressure: implications for the Earth, Science 275 (1997) 654–657.